ACS APPLIED MATERIALS & INTERFACES

Research Article

www.acsami.org

In Situ Ion Exchange Synthesis of Strongly Coupled Ag@AgCl/g-C_3N_4 Porous Nanosheets as Plasmonic Photocatalyst for Highly Efficient Visible-Light Photocatalysis

Shouwei Zhang,[†,‡] Jiaxing Li,[*,†,∥] Xiangke Wang,[*,†,§,∥,⊥] Yongshun Huang,[†] Meiyi Zeng,[‡] and Jinzhang Xu[‡]

[†]School of Environment and Chemical Engineering, North China Electric Power University, Beijing 102206, P. R. China

[‡]School of Materials Science and Engineering, Hefei University of Technology, Hefei 230031, P. R. China

[§]Faculty of Engineering, King Abdulaziz University, Jeddah 21589, Saudi Arabia

[∥]Collaborative Innovation Center of Radiation Medicine of Jiangsu Higher Education Institutions, Jiangsu, P. R. China

[⊥]School for Radiological and interdisciplinary Sciences (RAD-X), Soochow University, 215123 Suzhou, P. R. China

Supporting Information

ABSTRACT: A novel efficient Ag@AgCl/g-C_3N_4 plasmonic photocatalyst was synthesized by a rational *in situ* ion exchange approach between exfoliated g-C_3N_4 nanosheets with porous 2D morphology and $AgNO_3$. The as-prepared Ag@AgCl-9/g-C_3N_4 plasmonic photocatalyst exhibited excellent photocatalytic performance under visible light irradiation for rhodamine B degradation with a rate constant of 0.1954 min^{-1}, which is ~41.6 and ~16.8 times higher than those of the g-C_3N_4 (~0.0047 min^{-1}) and Ag/AgCl (~0.0116 min^{-1}), respectively. The degradation of methylene blue, methyl orange, and colorless phenol further confirmed the broad spectrum photocatalytic degradation abilities of Ag@AgCl-9/g-C_3N_4. These results suggested that an integration of the synergetic effect of suitable size plasmonic Ag@AgCl and strong coupling effect between the Ag@AgCl nanoparticles and the exfoliated porous g-C_3N_4 nanosheets was superior for visible-light-responsive and fast separation of photogenerated electron−hole pairs, thus significantly improving the photocatalytic efficiency. This work may provide a novel concept for the rational design of stable and high performance g-C_3N_4-based plasmonic photocatalysts for unique photochemical reaction.

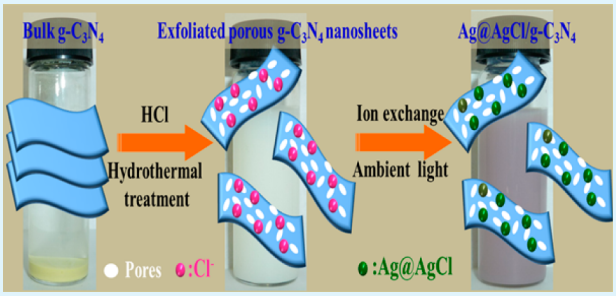

KEYWORDS: *plasmonic photocatalyst, Ag@AgCl/g-C_3N_4, heterostructures, ion exchange, visible light, photocatalysis*

1. INTRODUCTION

Environmental pollution has become one of the arduous challenges to the sustainable development of modern human society. Recently, the "green-life" concept is inspiring enthusiasm to exploit the novel, "zero" waste scheme and eco-friendly photocatalysts for air purification and wastewater cleaning. As a "green" method, the semiconductor photocatalytic degradation of organic pollutants has attracted extensive attention because they can eliminate most organic contaminants.[1−3] Visible-light energy (~48% of the solar spectrum) within solar spectra is far more abundant than UV energy (~4% of the solar spectrum).[4] Therefore, the development of visible-light-responsive photocatalysts for efficient utilization of the sunlight has gained much attention. Meanwhile, a high performance photocatalyst should possess good separation of electron−hole pairs.[5,6] Hence, the construction of suitable structures within highly interactive interfaces is of vital importance to achieve effective separation of photogenerated charges and to extend absorption spectrum.

Recently, two-dimensional (2D) materials have been widely studied due to their unique structural and optical properties, of which the g-C_3N_4 material gained special attractions because of its abundant, suitable bandgap and high chemical stability, making it potentially suitable for solar energy conversion, oxygen reduction, and environment purification.[7−10] However, the photocatalytic performance of g-C_3N_4 is far from satisfactory due to its high photogenerated charge recombination rate and low absorption efficiency above 460 nm in sunlight spectra.[11] Various chemical strategies have been applied to improve photogenerated charge separation and to extend light absorption of g-C_3N_4, such as nano/mesoporous structure fabrication by hard or soft template approach, copolymerization, semiconductor modification, metal and/or nonmetal doping, etc.[12] However, poor light absorption capacity and quantum efficiency remained in these modified

Received: August 18, 2014
Accepted: November 26, 2014
Published: November 26, 2014

g-C_3N_4 systems. Therefore, it is still necessary to find a reasonable strategy to further improve the photocatalytic properties of g-C_3N_4-based photocatalysts.

Many novel advanced photocatalysts have been designed on the basis of surface plasmon resonance (SPR) of metal nanoparticles.[13] An example involved the plasmonic photocatalysts, which displayed excellent plasmonic photocatalytic performance under visible light irradiation for pollutant degradation, water disinfection, and carbon dioxide reduction.[13−16] Ingram et al. had designed a novel plasmonic metal/semiconductor (Ag/N-TiO_2) photocatalyst, which displayed enhanced visible-light photocatalytic activity as compared to the semiconductor alone.[17] Zheng et al. developed a facile *in situ* method to prepare noble-metal plasmonic photocatalysts M@TiO_2 (M = Au, Pt, or Ag), which could selectively oxidize benzene to phenol with a high yield.[18] Commercially, Ag-based plasmonic photocatalysts are more practical due to their relatively low price. Xu et al. prepared AgX/g-C_3N_4 (X = Br or I) composites with high photocatalytic activities in methyl orange (MO) degradation.[11] Ma et al. synthesized Ag-AgCl-WO_3 hollow spheres to photocatalytically degrade 4-chlorophenol.[19] Enhanced photocatalytic activity for MO degradation was observed by graphene oxide (GO)-hybridized 1D Ag/AgCl nanocomposites, as reported by Zhu et al.[20] Huang's group developed a series of Ag/AgX (X = Cl or Br) plasmonic photocatalysts, which had strong absorption in the visible region and showed high efficiencies in the photodegradation of organic pollutants.[21−23] These studies clearly indicated the increasing photocatalytic activities by incorporating AgX with other semiconductors, of which Ag/AgCl nanomaterials showed superior plasmonic photocatalytic activities to degrade pollutants under visible-light irradiation.[24,25] This might be attributed to the metallic Ag nanoparticles, which could significantly expand light response range to visible light region and could effectively promote photogenerated charge separation/transfer.[25] However, the AgX species, prepared from traditional methods, always suffer from decomposition under sunlight irradiation, resulting in poor photocatalytic activities. Besides, Ag nanoparticles produced by AgX usually form large and disordered particles, which adversely affect their SPR effect that relies on the shape, size, and distribution of the noble metal.[26] Ion exchange approach had been widely used in the synthesis of hybrid composites. For example, Li et al. reported a rapid, facile, and scalable method to fabricate a series of silver nanotubes Ag_nX, such as Ag_2S, AgCl, Ag_3PO_4, and $Ag_2C_2O_4$, from pregrown Ag_2CO_3 nanorods via a rapid acid-etching anion exchange process.[27] $AgVO_3$@AgBr@Ag nanobelt heterostructures were fabricated as an efficient visible-light photocatalyst through an anion exchange reaction, which displayed a high performance to remove organic dye in the range of visible light.[28] ZnS:Ag_2S porous nanostructures were prepared by a simple ion exchange route, using ZnS nanosheets as sacrificial templates, with controllable pore sizes by adjusting the concentration of Ag ions.[29] The above discussions clearly indicated the advantages of ion exchange method, such as low cost, simplicity, controllable porous size, and high contact extent between composite phases.[14,27,30,31]

Herein, in continuation of our interest in the g-C_3N_4-based nanomaterials,[32−35] we prepared novel visible-light-driven plasmonic photocatalyst, Ag@AgCl/g-C_3N_4, as porous nanosheet composites (defined as Ag@AgCl/CN) via ion exchange approach. To the best of our knowledge, the synthesis of g-C_3N_4-based plasmonic photocatalysts by protonated g-C_3N_4 as a precursor through ion exchange approach has never been reported, especially for their applications to degrade organic pollutants by visible-light photocatalysis. The experimental results showed that the as-prepared Ag@AgCl/CN plasmonic photocatalysts exhibited superior photocatalytic activities in decomposing organic pollutants under visible light irradiation. This strategy might provide a new route to develop new series of stable and high efficient g-C_3N_4-based plasmonic photocatalysts.

2. EXPERIMENTAL SECTION

2.1. Synthesis of Exfoliated Porous g-C_3N_4 Nanosheets. Bulk g-C_3N_4 was prepared by heating melamine to 550 °C for 4 h with a ramping rate of 2.5 °C/min. The typical exfoliated process was undertaken by stirring bulk g-C_3N_4 (320 mg) in 6 M HCl solution (80 mL). The mixed solution was then transferred into 80 mL Teflon and heated in a sealed autoclave at 110 °C for 5 h. Upon cooling to room temperature, the precipitate was purified by repeated centrifugation, dispersion, and ultrasonication until neutral solution was obtained. Finally, the exfoliated porous g-C_3N_4 nanosheets were obtained by drying at 80 °C under vacuum overnight.

2.2. Synthesis of Ag@AgCl/CN Plasmonic Photocatalysts. The Ag@AgCl/CN plasmonic photocatalysts were synthesized by *in situ* ion exchange approach. Exfoliated porous g-C_3N_4 nanosheets (50 mg) were dispersed in a mixed solution of 80 mL of ethylene glycol and 0.9 mmol of $AgNO_3$. This solution was stirred vigorously. The obtained sample, defined as Ag@AgCl-9/CN, was washed and dried. Samples Ag@AgCl-3/CN, Ag@AgCl-6/CN, and Ag@AgCl-12/CN were prepared similarly to Ag@AgCl-9/CN by changing the initial amount of $AgNO_3$ to be 0.3, 0.6, and 1.2 mmol, respectively. For comparison, two controlled samples were also prepared. The Ag@AgCl-9 was prepared by the following procedure. An excess of NaCl solution (0.1 mol/L) was added dropwise into 0.9 mmol of $AgNO_3$ (100 mL) with vigorous stirring. After stirring for 6 h, the precipitate was washed by water and alcohol several times, and dried under 40 °C. The other one was made by direct precipitation of 0.9 mmol of $AgNO_3$, NaCl, and 50 mg of g-C_3N_4, defined as dp-Ag@AgCl-9/CN.

2.3. Photocatalytic Degradation of Dyes and Phenol. Rhodamine B (RhB), methylene blue (MB), methyl orange (MO), and colorless phenol were selected as model pollutants for degradation experiments under visible-light irradiation. The visible-light was obtained from a 300 W Xe lamp, equipped with a super cold filter, which provided the visible-light region from 400 to 700 nm. The distance between the light source and the reactor was ∼5 cm. The aqueous suspensions were irradiated in an 150 mL open cylindrical reactor whose base contained an optical window with a surface area of ∼100 cm^2 and an average light intensity of ∼90 mW/cm^2. The photocatalytic activities of the photocatalysts (25 mg) were examined by monitoring the degradation of dyes (10 mg/L, 100 mL) in a beaker under stirring condition (400 rpm/min) at room temperature. The mixtures were prestirred for ∼3 h in the dark to ensure adsorption equilibrium. The absorption spectra were recorded on a UV−vis spectrophotometer (UV-2550, Shimadzu).

2.4. Characterization. The as-prepared photocatalysts were characterized by X-ray diffraction (XRD) for phase identification on a D/MAX2500 V diffractometer using Cu Kα radiation. The morphologies of photocatalysts were observed by field emission transmission electron microscope (TEM, JEOL-2100). X-ray photoelectron spectroscopy (XPS) data were obtained with an ESCA Lab220i-XL electron spectrometer from VG Scientific using 300W Al Kα radiation. The Brunauer−Emmett−Teller (BET) N_2 adsorption analysis was conducted on an ASAP 2020 physisorption analyzer. The pore-size distributions of the samples were also estimated using the Barrett−Joyner−Halenda (BJH) method. UV−vis diffuse reflection spectroscopy (DRS) was performed on a Shimadzu UV-2500 spectrophotometer using $BaSO_4$ as the reference.

Scheme 1. Schematic Route for the Synthesis of Ag@AgCl/g-C_3N_4 Plasmonic Photocatalysts

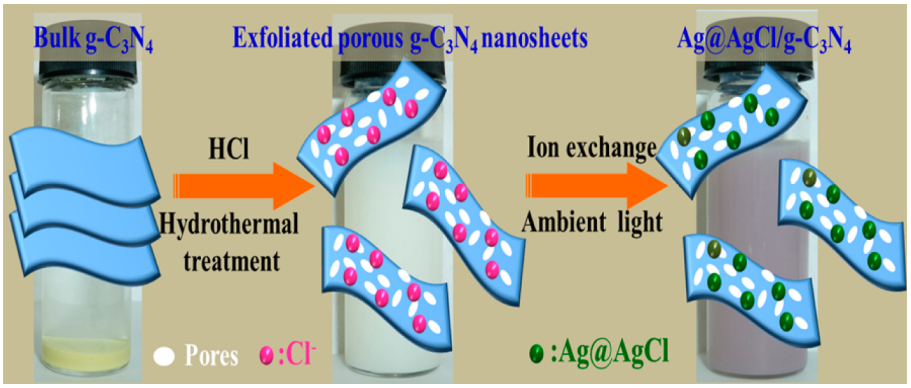

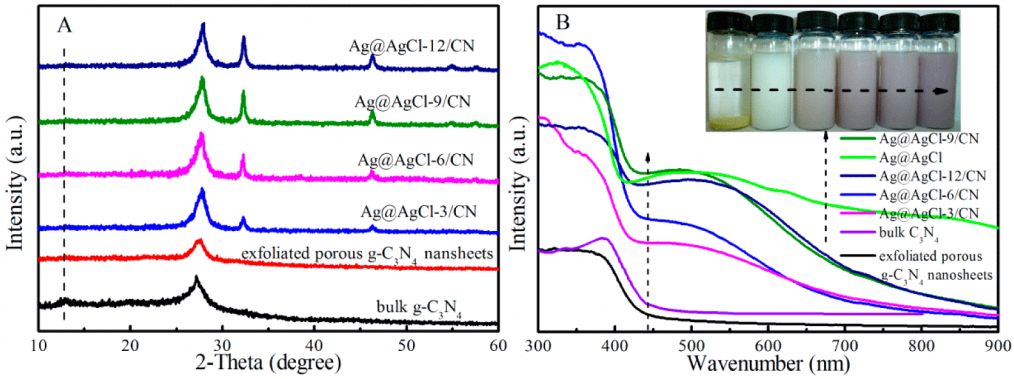

Figure 1. XRD patterns (A) and UV−vis diffuse reflectance spectra (B) of as-prepared photocatalysts.

3. RESULTS AND DISCUSSION

The fabrication of Ag@AgCl/CN plasmonic photocatalysts is shown in Scheme 1 via a two-step strategy. Exfoliated porous g-C_3N_4 nanosheets were first prepared by an acid-assisted hydrothermal method, followed by successful deposition of AgCl nanoparticles (as nanoislands) on the surface of exfoliated porous g-C_3N_4 nanosheets by ion exchange approach with high dispersity. Meanwhile, AgCl nanoparticles were partially reduced to Ag^0 by the nature light to obtain the desired Ag@AgCl/CN plasmonic photocatalysts.[36]

3.1. Material Characterization. The XRD patterns of bulk g-C_3N_4, exfoliated porous g-C_3N_4 nanosheets, and the as-prepared photocatalysts are collected in Figure 1A. A typical interplanar stacking peak in conjugated aromatic systems was observed for both bulk g-C_3N_4 and exfoliated porous g-C_3N_4 nanosheets. The peak shift from 27.21° to 27.89° corresponded to a decreased interplanar stacking distance from 0.326 to 0.319 nm. This result indicated a decreased gallery distance between the layers in the carbon nitride, demonstrating the successful exfoliation between the layered g-C_3N_4 during the acid-assisted hydrothermal process.[37] For Ag@AgCl/CN plasmonic photocatalysts, the diffraction peaks at 32.34°, 46.31°, 54.96°, and 57.6° could be indexed to the (200), (220), (311), and (222) planes, respectively, which agreed with the face-centered cubic AgCl (JCPDS file: 31-1238),[38] and the peak intensities increased with the increasing $AgNO_3$ content. The peak located at ~27.96° could be an overlap of (111) plane of AgCl (2θ = ~27.58°) and (200) plane of g-C_3N_4 (2θ = ~27.89°), resulting in the increment of intensity and decrement of full width at half-maximum, as compared with exfoliated porous g-C_3N_4 nanosheets. In addition, the low-angle diffraction peak at 13.3° (d = 0.663 nm), derived from in-planar repeated tri-s-triazine units, disappeared for the exfoliated porous g-C_3N_4 nanosheets due to the simultaneously decreased planar size of the CN layers after protonation and exfoliation. No obvious diffraction peaks were observed for Ag^0, probably due to its small size or high dispersity, which is in agreement with the previous report.[31] In addition, the particle sizes of Ag@AgCl/CN composites were calculated from Scherrer formula, as shown in Supporting Information Table S1. As disscussed above, the Ag@AgCl/CN composites were successfully fabricated by the facile ion exchange approach.

The UV−vis spectra of the Ag@AgCl/CN plasmonic photocatalysts are shown in Figure 1B. The absorption edge of the exfoliated porous g-C_3N_4 nanosheets indicated a slight blue shift as compared with the bulk g-C_3N_4. In contrast to exfoliated porous g-C_3N_4 nanosheets with absorption edge at ~450 nm, the absorption intensities of Ag@AgCl/CN composites became stronger in the whole interested spectrum window, especially in the visible-light region, due to the strong SPR absorption of Ag nanocrystals.[31,36,38] In addition, the absorption spectra were largely red-shifted, and a broad absorption ranging from ~450 to ~800 nm was detected. Accordingly, the suspension color was also changed from milky to pink, indicating the generation of Ag nanocrystals (Figure 1B).[39] Obviously, the introduction of Ag@AgCl can significantly enhance the absorption in the visible-light region and can even extend to near-infrared region, which is attributed to the SPR of Ag nanoparticles.

The chemical compositions of the as-prepared plasmonic photocatalysts are characterized by XPS spectra, as shown in Figure 2. The successful modification of the g-C_3N_4 suface by

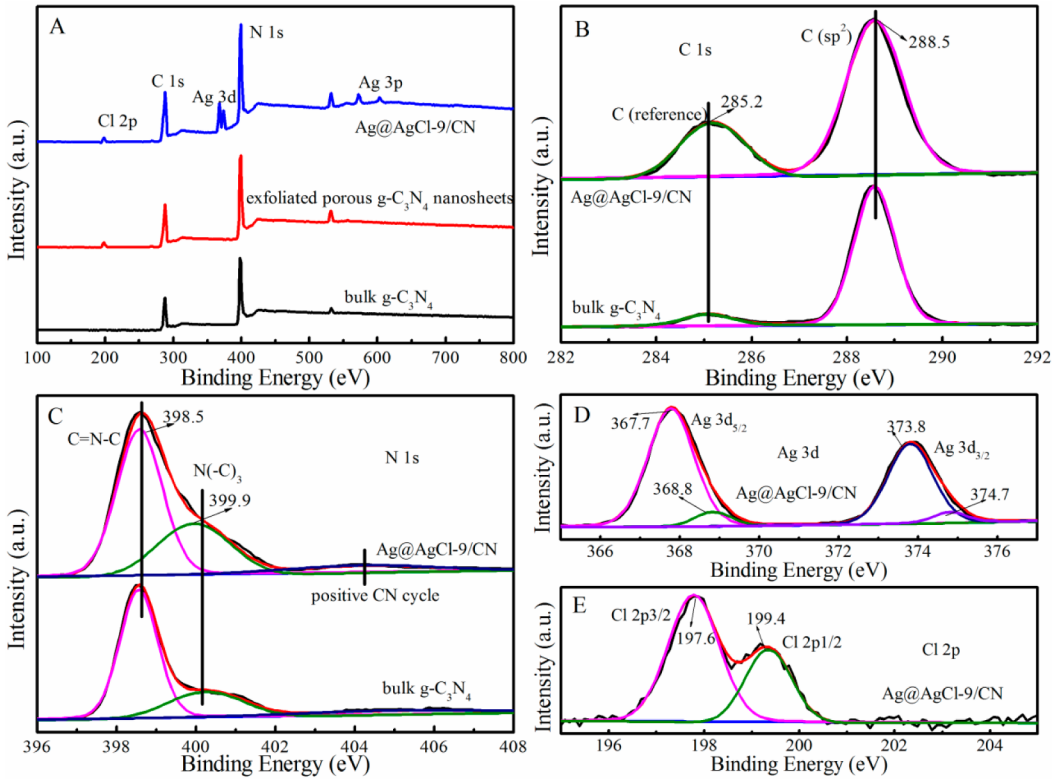

Figure 2. XPS survey spectra (A) of as-prepared photocatalysts, high resolution C 1s (B) and N 1s (C) spectra of bulk g-C_3N_4 and Ag@AgCl-9/CN, and high resolution Ag 3d (D) and Cl 2p (E) spectra of Ag@AgCl-9/CN.

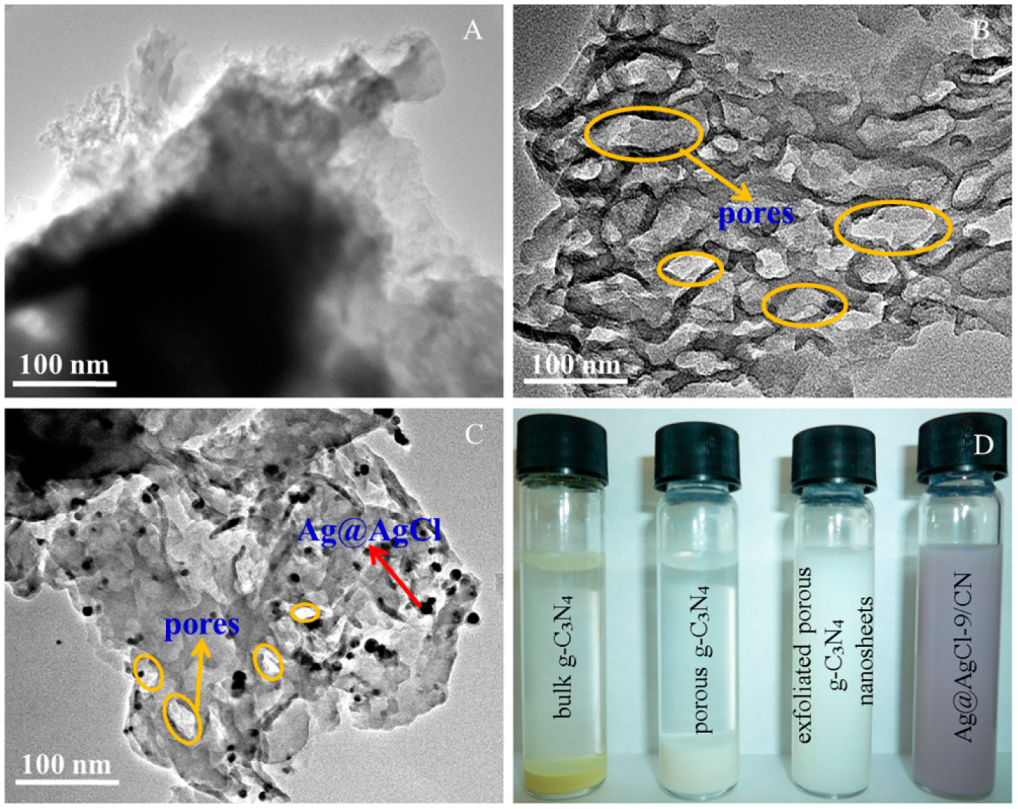

Figure 3. TEM images of bulk g-C_3N_4 (A), exfoliated porous g-C_3N_4 nanosheets (B) and Ag@AgCl-9/CN (C), and the dispersion photographs of the as-prepared photocatalysts in water for 72 h (D).

acid-assisted hydrothermal treatment was confirmed by the new existing Cl peak in the survey spectrum of exfoliated porous g-C_3N_4 nanosheets (Figure 2A). As for Ag@AgCl-9/CN, new Ag peaks were observed, confirming the decoration of the Ag@

dx.doi.org/10.1021/am505528c | ACS Appl. Mater. Interfaces 2014, 6, 22116−22125

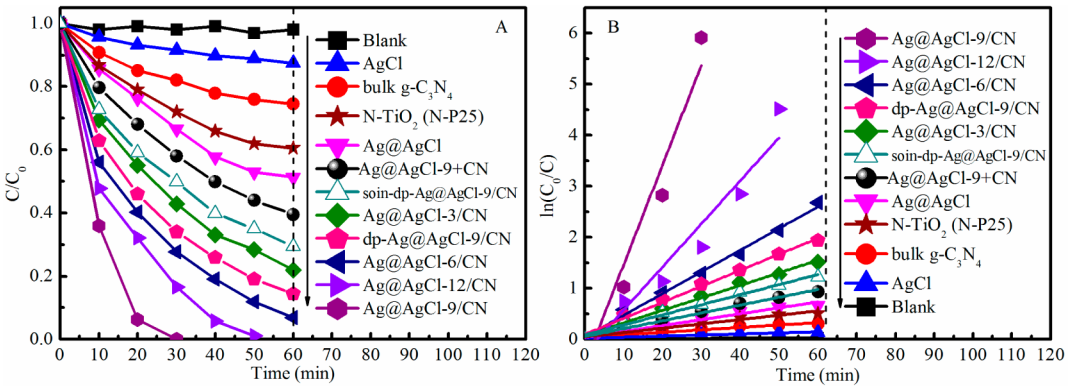

Figure 4. Photocatalytic degradation of RhB by the as-prepared photocatalysts under visible light irradiation (A) and kinetic fit for MB degradation by the as-prepared photocatalysts (B).

AgCl nanoparticles on the exfoliated porous g-C_3N_4 surface. The high resolution C 1s spectra can be divided into two peaks located at ~285.2 and ~288.5 eV, being ascribed to the standard reference carbon and the sp^2-bonded carbon (N—C═N), respectively (Figure 2B).[37,40] For high resolution N 1s spectra (Figure 2C), the peaks centered at ~398.5 and ~399.9 eV belonged to the sp^2-hybridized aromatic N atoms bonded to carbon atoms (C—N═C) and the tertiary N atoms bonded to carbon atoms in the form of N(—C)$_3$, respectively.[37] The emerging peak at ~404.2 eV corresponded to the charging effects or positive charge localization in heterocycles or the cyano functional groups, which originated from the protonation of g-C_3N_4 nanosheets.[37] For Ag@AgCl (Supporting Information Figure S1), two bands at ca. 367.5 and 373.5 eV were observed, which were ascribed to Ag $3d_{5/2}$ and Ag $3d_{3/2}$ binding energies, respectively. In the case of Ag@AgCl-9/CN, the high resolution XPS data of Ag 3d peaks are shown in Figure 2D. Two peaks of Ag 3d located at ~367.7 and ~373.8 eV were attributed to the Ag $3d_{5/2}$ and Ag $3d_{3/2}$ binding energies, respectively.[31,41] These two bands could be further deconvoluted into two peaks. The peaks located at ~367.7 and ~373.8 eV were ascribed to Ag^+ in AgCl, and the peaks centered at ~368.8 and ~374.7 eV belonged to the metallic Ag^0 species.[16] In addition, the surface Ag^0 content (mole ratio of Ag^0 to Ag^0 + Ag^+) was semiquantitatively estimated by the XPS Ag 3d peak area analysis and summarized in Supporting Information Table S2. These results further corroborated the existence of metallic Ag^0 in Ag@AgCl-9/CN, as suggested by the UV–vis spectra. The spectrum of Cl 2p (Figure 2E and Supporting Information Figure S10) displayed double peaks located at ~197.6 and ~199.4 eV, which could be assigned to the characteristic doublets of Cl $2p_{3/2}$ and Cl $2p_{1/2}$, respectively.[36]

Typical morphologies of the as-prepared plasmonic photocatalysts are shown in Figure 3. Bulk g-C_3N_4 was presented as irregular thick block material (Figure 3A), while pores can be observed on the surface of the exfoliated porous g-C_3N_4 nanosheets after acid-assisted hydrothermal treatment (Figure 3B). Black Ag@AgCl nanoparticles (~8–12 nm) (as nanoislands) were uniformly deposited on the surface of exfoliated porous g-C_3N_4 nanosheets, as depicted in Figure 3C of the morphology of Ag@AgCl-9/CN plasmonic photocatalyst.[6] The HRTEM image of the Ag@AgCl-9/CN was displayed in Supporting Information Figure S2. By measuring the lattice fringes, the lattice distance of 0.23 and 0.32 nm corresponded to the (111) plane of cubic Ag^0 and the (111) plane of cubic AgCl, respectively. Besides, the HRTEM image clearly revealed a close interface between Ag^0 and AgCl in the as-prepared composite with the formation of heterojunction, which is important for the separation of the photogenerated electron–hole pairs to improve the quantum efficiency. The high dispersity of Ag@AgCl nanoparticles was expected to provide more active sites and to offer enhanced photocatalytic performances.[6] To further confirm the porous structures in the hybrid material, the BET surface area and BJH pore size distribution were measured to provide concrete evidence (Supporting Information Figure S3). Meanwhile, the formation mechanism of the porous structure was presented in Supporting Information Figure S4. The strong coupling effect between the Ag@AgCl nanoparticles and the exfoliated porous g-C_3N_4 nanosheets was confirmed by ultrasonicating and stirring for 24 h in ethanol solution with no observed dropped off Ag@AgCl nanoparticles. On the contrary, the Ag@AgCl particles on the dp-Ag@AgCl/CN surface were peeled off after ultrasonication, which was defined as soin-dp-Ag@AgCl-9/CN (Supporting Information Figure S5). Figure 3D displayed the dispersion photographs of the as-prepared photocatalysts in water for 72 h under ambient conditions. The porous g-C_3N_4 was produced by partially acidic protonation of bulk g-C_3N_4 (Supporting Information Figure S6), and the precipitation can be observed after a couple of 10 min periods (Figure 3D). By hydrothermal treatment in the presence of hydrochloric acid, highly dispersed exfoliated porous g-C_3N_4 nanosheets were obtained. The dispersion photographs clearly demonstrated that exfoliated porous g-C_3N_4 nanosheets and Ag@AgCl-9/CN could be easily dispersed in water to form a stable dispersion without visible sedimentation, which could significantly facilitate the surface contact between the photocatalysts and the organic pollutants to improve the photocatalytic performance.

3.2. Photocatalytic Performances. RhB was selected to test the photocatalytic performances of the as-prepared Ag@AgCl/CN photocatalysts under visible-light irradiation ($\lambda > 400$ nm), as collected in Figure 4A. No noticeable RhB degradation was observed by direct photolysis without any photocatalysts, indicating negligible direct photolysis of RhB in our case.[6] Only ~12% and ~26% RhB were degraded by AgCl and bulk g-C_3N_4 within 60 min, indicating the poor photocatalytic activities. Among all the as-prepared photocatalysts, Ag@AgCl-9/CN exhibited the highest photocatalytic degradation efficiency, on which RhB was almost quantitatively degraded within 30 min. In comparison, the corresponding degradation efficiencies were ~33.5%, ~57.2%, ~72.4%, and ~83.5% for Ag/AgCl, Ag@

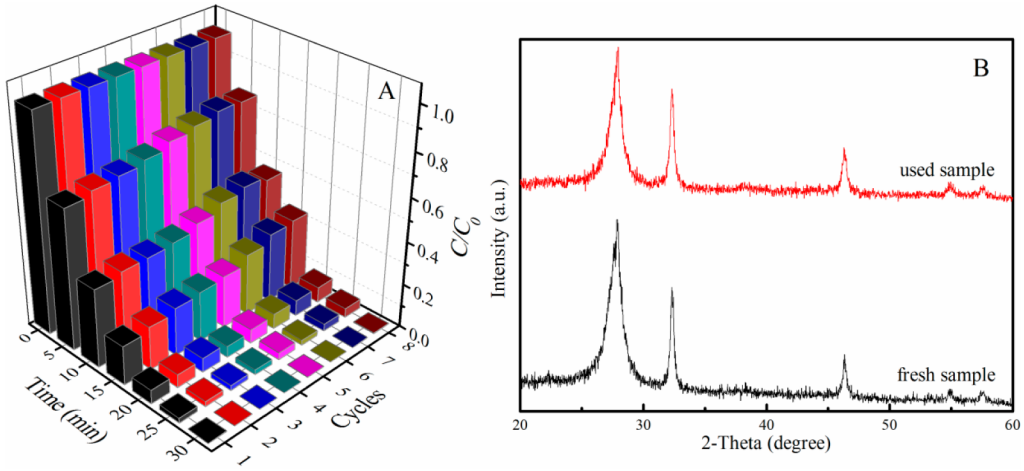

Figure 5. Recycle tests (A) and XRD patterns (B) of Ag@AgCl-9/CN under visible light irradiation.

AgCl-3/CN, Ag@AgCl-6/CN, and Ag@AgCl-12/CN, respectively. This observation clearly illustrates the importance of the amount of Ag@AgCl in the Ag@AgCl/CN composites to the photocatalytic performances, which meant that the photocatalytic performances of the Ag@AgCl/CN photocatalysts depended on the interaction among AgCl, Ag, and g-C_3N_4. For the system of Ag@AgCl in Ag@AgCl/CN composites, the charge distribution of Ag nanoparticles may change due to the polarization interaction by AgCl, resulting in partial negative and positive charged regions in the Ag nanoparticles that are far from and close to the Ag/AgCl interface, respectively.[24,39] In addition, driven by the polarization field around AgCl, the excited electrons on the surface of Ag nanoparticles can force away from the interfaces and prevent photoreduction of AgCl to Ag under visible-light illumination.[24,39] That is, synergistic effect between the improved absorption of visible light by strong SPR of the Ag nanoparticles and polarization field provided by the AgCl facilitates photogenerated charge separation and interfacial transfer. For the system of AgCl/CN in Ag@AgCl/CN nanocomposites, the strong heterojunction effect was formed on the interface between g-C_3N_4 nanosheets and AgCl due to its suitable band gap, which would accelerate the photogenerated charge effective separation and transfer, resulting in superior photocatalytic activities. Furthermore, another possible reason for the superior photocatalytic performances of the as-prepared photocatalysts with suitable ratio and size of Ag nanoparticles were their SPR absorption over a wider visible light.[39] The coupling effect between the Ag@AgCl and g-C_3N_4 nanosheet would be weakened with increasing amount of Ag@AgCl (such as Ag@AgCl-12/CN), which may damage the heterojunction interfaces, resulting in a decreased efficiency of photogenerated charge separation and transfer (Supporting Information Figure S7).[42] Therefore, the superior photocatalytic performance of Ag@AgCl-9/CN may be attributed to its high dispersion and suitable size of Ag@AgCl on the exfoliated porous g-C_3N_4 nanosheet surface. However, a further increment deposition (Ag@AgCl-12/CN) could result in negative effects toward the photocatalytic efficiency. In conclusion, an appropriate size and dispersion of Ag@AgCl on g-C_3N_4 nanosheets were important for the enhancement of the photocatalytic activity.

A physical mixture of Ag/AgCl-9 and g-C_3N_4 (defined as Ag/AgCl-9+CN) was also tested for RhB degradation, which exhibited much weaker photocatalytic activity as compared with Ag@AgCl-9/CN. This observation further corroborated the importance of strong coupling heterojunction interface between Ag@AgCl and g-C_3N_4 to the effective photogenerated charge separation and transfer.[43] The lower photocatalytic activity of dp-Ag@AgCl-9/CN was also observed, which could be ascribed to the weak interactions between Ag@AgCl and g-C_3N_4 and large particle size of Ag@AgCl in dp-Ag@AgCl/CN by the directly precipitation, as shown in Supporting Information Figure S7D. This clearly illustrated the advantages of ion exchange strategy over the directly precipitation to form strong coupling interaction and to control the particle sizes of Ag@AgCl. The weak interactions between Ag@AgCl and g-C_3N_4 in dp-Ag@AgCl-9/CN were tested by ultrasonicating for about 5 h to obtain soni-dp-Ag@AgCl-9/CN (Supporting Information Figure S5), which exhibited an even lower degradation efficiency of ~72.6% within 60 min (Figure 4A). Therefore, in order to obtain high efficient photocatalytic activity, a suitable particle size, high dispersity, and a strong coupling heterostructure of Ag@AgCl/CN should be achieved to accelerate photogenerated electron−hole pair separation and transfer.

The UV−vis spectra change during the RhB photodegradation by Ag@AgCl-9/CN is collected in Supporting Information Figure S8. A decreased absorption intensity at the maximum absorption wavelength of RhB (λ = 553 nm) was observed, as well as a blue shift in the absorption band, indicating a dominant de-ethylation process.[24] The disappearance of the characteristic absorption peak of RhB within 30 min indicated an excellent photocatalytic degradation activity of the Ag@AgCl-9/CN toward RhB under visible-light irradiation.

To quantitatively investigate the reaction kinetics of RhB photodegradation by the as-prepared photocatalysts, the experimental data were analyzed by the pseudo-first-order kinetic model

$$\ln\left(\frac{C_0}{C}\right) = Kt \quad (1)$$

where K is the rate constant (min^{-1}), C_0 is the initial concentration of RhB, and C is the concentration of RhB at time t. Linear relationships were obtained as depicted in Figure 4B, which indicated that the RhB photodegradation process can be fitted by the pseudo-first-order model well. The highest photocatalytic degradation rate was obtained by Ag@AgCl-9/CN to be 0.1954 min^{-1}, which was ~41.6, ~16.8, ~8.0, ~4.6,

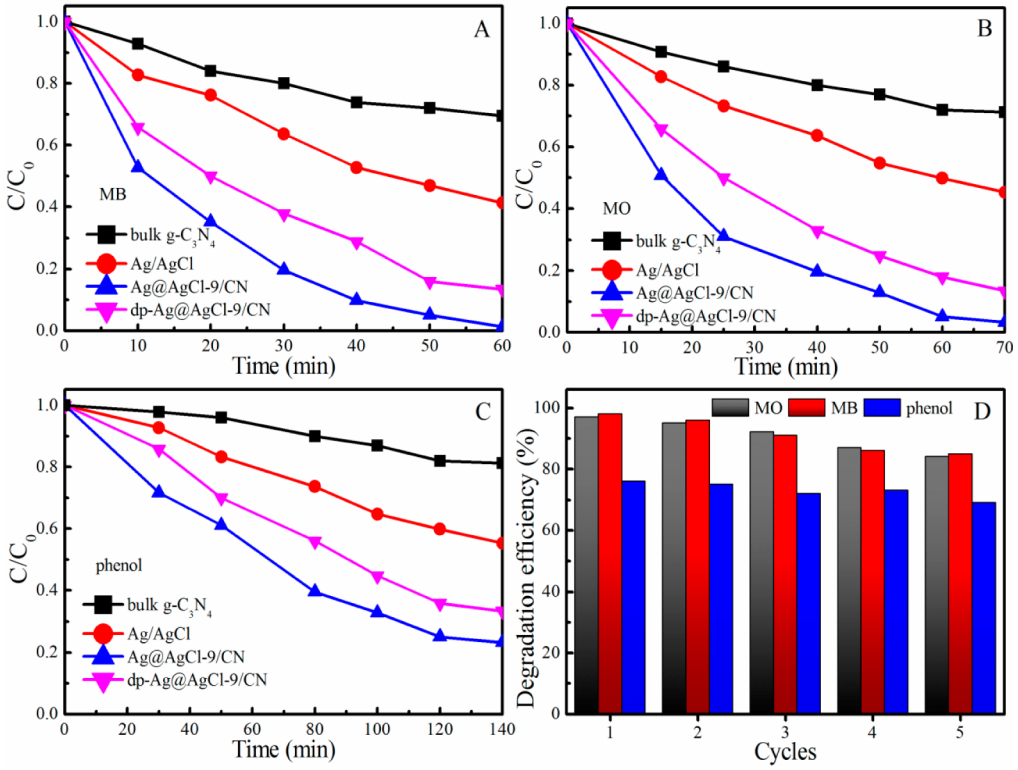

Figure 6. Photocatalytic degradation of MB (A), MO (B), and colorless phenol (C) in the presence of different photocatalysts under visible-light irradiation; the corresponding recycle test for different dyes in the presence of Ag@AgCl-9/CN under visible-light irradiation (D).

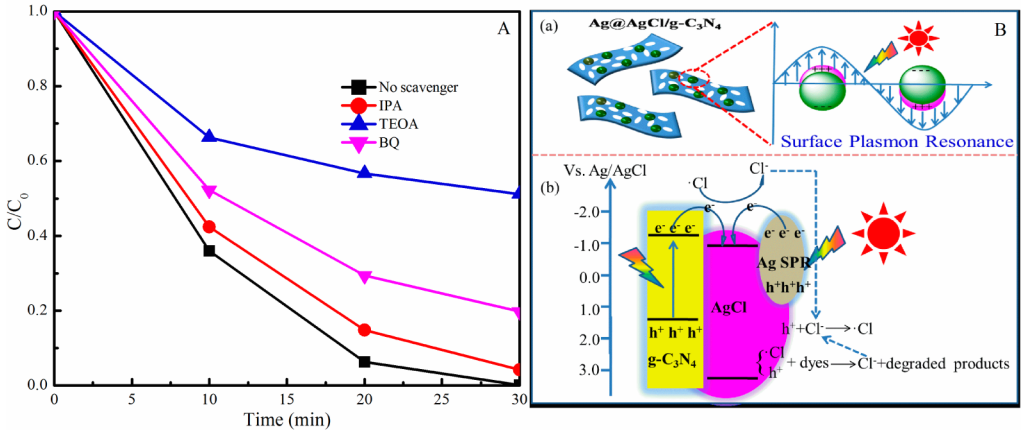

Figure 7. Effect of different scavengers on the RhB degradation in the presence of Ag@AgCl-9/CN (A) and a proposed schematic mechanism for photocatalytic reactions on Ag@AgCl-9/CN surface under visible-light irradiation (B).

~2.3 times faster than those of the bulk g-C_3N_4 (~0.0047 min^{-1}), Ag/AgCl (0.0116 min^{-1}), Ag@AgCl-3/CN (0.0244 min^{-1}), Ag@AgCl-6/CN (0.0424 min^{-1}), and Ag@AgCl-12/CN (0.0843 min^{-1}), respectively. Besides the excellent photocatalytic efficiency, the reusability and stability of Ag@AgCl-9/CN were also tested for practical applications (Figure 5). The good reusability can be confirmed by the consistent photocatalytic activity even after eight cycles (Figure 5A). The stability of the used samples was examined by the XRD patterns. A lower Ag^0 peak may be attributed to photocorrosion of the Ag@AgCl-9/CN (Figure 5B). That is, the stability experiment results confirmed that the Ag@AgCl-9/CN plasmonic photocatalyst exhibited broad spectrum photocatalytic degradation ability and stability, but the inevitable presence of photocorrosion in the case of long working hours.

The broad spectrum photocatalytic abilities of Ag@AgCl-9/CN were further investigated by degrading MB, MO, and phenol as pollutants (Figure 6). The highest photocatalytic degradation efficiencies were also observed by Ag@AgCl-9/CN as compared with other photocatalysts. The degradation process can be finished within 60 and 70 min for MB and MO, respectively (Figure 6A,B). To rule out photosensitization effect under visible-light irradiation,[44] we also evaluated the photocatalytic performance of Ag@AgCl-9/CN toward the colorless phenol (Figure 6C). As expected, Ag@AgCl-9/CN also exhibited the highest photocatalytic performance for phenol degradation. The stability and recyclability of Ag@AgCl-9/CN to MB, MO, and phenol degradation were also examined with no significant reduction after five cycles (Figure 6D). The structure of the used sample remained the same

except an extremely weak peak of Ag^0, which may also be caused by photocorrosion (Figure 5B and Supporting Information Figure S9). These results indicated that the Ag@AgCl-9/CN plasmonic photocatalyst was an efficient visible-light-driven photocatalyst with broad photocatalytic spectrum, good reusability, and stability for potential practical applications in wastewater treatment.

The photocatalytic degradation mechanism of dye pollutants by the Ag@AgCl-9/CN plasmonic photocatalysts was systematically investigated by introducing isopropyl alcohol (IPA), triethanolamine (TEOA), and *p*-benzoquinone (BQ), which are known as effective $^{\bullet}OH$, holes, and $^{\bullet}O_2^-$ scavengers for photocatalytic reaction, respectively (Figure 7A).[45] Meanwhile, to further confirm the presence of superoxide radicals ($^{\bullet}O_2^-$), a certain amount of O_2 was introduced. All scavengers were observed to partially suppress the photodegradation rates as compared to the absence of scavengers. The photodegradation rates decreased in the order TEOA < BQ < IPA, indicating that h^+ and $^{\bullet}O_2^-$ are the main oxidative species in the photocatalytic process with a major species of h^+. The generation of $^{\bullet}O_2^-$ radicals in the photocatalytic process was confirmed by the DMPO-ESR technique as the presence of the characteristic peaks of the DMPO−$^{\bullet}O_2^-$ adducts, as shown in Supporting Information Figure S11.

On the basis of the above results, a reasonable photocatalytic mechanism was proposed (Figure 7B). The g-C_3N_4 nanosheets can be excited by visible-light, while AgCl cannot.[45] The synergistic interaction between the SPR of metallic Ag and polarization field around AgCl can force the photogenerated electrons in Ag nanoparticles far away from the interfaces of Ag/AgCl under visible-light irradiation to facilitate photogenerated electron−hole pair separation and interfacial photogenerated charge transfer. In addition, both the matching energy bands (AgCl and g-C_3N_4) and heterostructure effects are favorable for photogenerated electron−hole pair separation at the interfaces. The Ag@AgCl nanoislands on the exfoliated g-C_3N_4 nanosheets provided more active centers by fully exposing the adjacent area of island−sheet interfaces to the pollutants. The separation and transfer of photogenerated charge were also facilitated by the small size of Ag@AgCl nanoparticles. During the photocatalytic process, the continuous consumption of separated photogenerated electron−hole pairs can enable continuous photocatalytic degradation. Due to the relative negative conduction band (CB) potential of AgCl (−0.09 eV vs NHE) to $O_2/^{\bullet}O_2^-$ (−0.046 eV vs NHE), electrons on CB of AgCl can react with O_2 to produce $^{\bullet}O_2^-$.[45] Meanwhile, the photogenerated holes had a great affinity to capture electrons from adsorbed dye molecules; thus, it can oxidize organic pollutants directly. The photogenerated holes can also oxidize Cl^- ions to $^{\bullet}Cl$, which are active radical species to oxidize RhB by the regeneration of Cl^- ions for the next catalytic cycle.[45] Therefore, the major active species for the photocatalytic degradation was identified as the holes and $^{\bullet}O_2^-$, which is consistent with the trapping experiments (Figure 7A).

4. CONCLUSION

In summary, we have successfully synthesized a series of efficient Ag@AgCl/g-C_3N_4 plasmonic photocatalysts via *in situ* ion exchange approach. A porous 2D morphology was observed with the decoration of discrete Ag@AgCl nanoparticles as nanoislands on the surface of exfoliated g-C_3N_4 nanosheets. The as-prepared Ag@AgCl/g-C_3N_4 plasmonic photocatalyst exhibited excellent photocatalytic activities to degrade RhB with a rate constant of 0.1954 min^{-1}, which was ∼41.6 and ∼16.8 times faster than those of g-C_3N_4 (∼0.0047 min^{-1}) and Ag/AgCl (0.0116 min^{-1}), respectively. Suitable particle size of Ag@AgCl, high dispersity, and strong coupling effects were identified as key elements for high photodegradation efficiency of the as-prepared photocatalysts. This study might provide a new perspective for the rational design of stable and high performance g-C_3N_4-based plasmonic photocatalysts via ion exchange method.

■ ASSOCIATED CONTENT

Supporting Information

Typical XPS spectra of the Ag@AgCl photocatalysts, the HRTEM image of the as-prepared photocatalyst, nitrogen sorption isotherm, and pore size distribution plot of bulk g-C_3N_4, porous g-C_3N_4, and Ag@AgCl-9/CN; the TEM images of Ag@AgCl-3/CN, Ag@AgCl-6/CN, Ag@AgCl-12/CN, and dp-Ag@AgCl-9/CN; and the temporal evolution of the UV−vis spectra during the RhB photodegradation, and so on. This material is available free of charge via the Internet at http://pubs.acs.org/.

■ AUTHOR INFORMATION

Corresponding Authors

*E-mail: lijx@ipp.ac.cn. Fax: +86-551-65591310. Phone: +86-551-65592788.

*E-mail: xkwang@ipp.ac.cn.

Notes

The authors declare no competing financial interest.

■ ACKNOWLEDGMENTS

We greatly appreciate the financial support from National Natural Science Foundation of China (21272236, 21225730, and 91326202), the Ministry of Science and Technology of China (2011CB933700), Chinese National Fusion Project for ITER (No. 2013GB110000), and the Jiangsu Provincial Key Laboratory of Radiation Medicine and Protection and the Priority Academic Program Development of Jiangsu Higher Education Institutions.

■ REFERENCES

(1) Zhang, H.; Fan, X.; Quan, X.; Chen, S.; Yu, H. Graphene Sheets Grafted Ag@AgCl Hybrid with Enhanced Plasmonic Photocatalytic Activity under Visible Light. *Environ. Sci. Technol.* **2011**, *45*, 5731−5736.

(2) Wang, W.; Du, H.; Wang, R.; Wen, T.; Xu, A. Heterostructured Ag_3PO_4/AgBr/Ag Plasmonic Photocatalyst with Enhanced Photocatalytic Activity and Stability under Visible Light. *Nanoscale* **2013**, *5*, 3315−3321.

(3) Ai, L.; Zhang, C.; Jiang, J. Hierarchical Porous AgCl@Ag Hollow Architectures: Self-templating Synthesis and Highly Enhanced Visible Light Photocatalytic Activity. *Appl. Catal., B* **2013**, *142*, 744−751.

(4) Jia, C.; Yang, P.; Huang, B. Uniform Ag/AgCl Necklace-Like Nano-Heterostructures: Fabrication and Highly Efficient Plasmonic Photocatalysis. *ChemCatChem* **2014**, *6*, 611−617.

(5) Di, J.; Xia, J.; Yin, S.; Xu, H.; Xu, L.; Xu, Y.; He, M.; Li, H. Preparation of Sphere-like g-C_3N_4/BiOI Photocatalysts via a Reactable Ionic Liquid for Visible-Light-Driven Photocatalytic Degradation of Pollutants. *J. Mater. Chem. A* **2014**, *2*, 5340−5351.

(6) Li, C.; Wang, S.; Wang, T.; Wei, Y.; Zhang, P.; Gong, J. Monoclinic Porous $BiVO_4$ Networks Decorated by Discrete g-C_3N_4 Nano-Islands with Tunable Coverage for Highly Efficient Photocatalysis. *Small* **2014**, *10*, 2783−2790.

(7) Wang, X.; Maeda, K.; Thomas, A.; Takanabe, K.; Xin, G.; Carlsson, J. M.; Domen, K.; Antonietti, M. A Metal-Free Polymeric Photocatalyst for Hydrogen Production from Water under Visible Light. *Nat. Mater.* **2008**, *8*, 76−80.
(8) Wang, X.; Blechert, S.; Antonietti, M. Polymeric Graphitic Carbon Nitride for Heterogeneous Photocatalysis. *ACS Catal.* **2012**, *2*, 1596−1606.
(9) Zhang, J.; Grzelczak, M.; Hou, Y.; Maeda, K.; Domen, K.; Fu, X.; Antonietti, M.; Wang, X. Photocatalytic Oxidation of Water by Polymeric Carbon Nitride Nanohybrids Made of Sustainable Elements. *Chem. Sci.* **2012**, *3*, 443−446.
(10) Cao, S.; Yu, J. g-C_3N_4 Based Photocatalysts for Hydrogen Production. *J. Phys. Chem. Lett.* **2014**, *5*, 2101−2107.
(11) Xu, H.; Yan, J.; Xu, Y.; Song, Y.; Li, H.; Xia, J.; Huang, C.; Wan, H. Novel Visible-Light-Driven AgX/graphite-like C_3N_4 (X =Br, I) Hybrid Materials with Synergistic Photocatalytic Activity. *Appl. Catal., B* **2013**, *129*, 182−193.
(12) Zhang, G.; Zhang, M.; Ye, X.; Qiu, X.; Lin, S.; Wang, X. Iodine Modified Carbon Nitride Semiconductors as Visible Light Photocatalysts for Hydrogen Evolution. *Adv. Mater.* **2014**, *26*, 805−809.
(13) Zhou, X.; Liu, G.; Yu, J.; Fan, W. Surface Plasmon Resonance-Mediated Photocatalysis by Noble Metal-based Composites under Visible Light. *J. Mater. Chem.* **2012**, *22*, 21337−21354.
(14) Fan, H.; Zhu, J.; Sun, J.; Zhang, S.; Ai, S. Ag/AgBr/Co-Ni-NO_3 Layered Double Hydroxide Nanocomposites with Highly Adsorptive and Photocatalytic Properties. *Chem.—Eur. J.* **2013**, *19*, 2523−2530.
(15) Zhang, D.; Li, G.; Jimmy, C. Y. Inorganic Materials for Photocatalytic Water Disinfection. *J. Mater. Chem.* **2010**, *20*, 4529−4536.
(16) An, C.; Wang, J.; Jiang, W.; Zhang, M.; Ming, X.; Wang, S.; Zhang, Q. Strongly Visible-Light Responsive Plasmonic Shaped AgX:Ag (X = Cl, Br) Nanoparticles for Reduction of CO_2 to Methanol. *Nanoscale* **2012**, *4*, 5646−5650.
(17) Ingram, D. B.; Christopher, P.; Bauer, J. L.; Linic, S. Predictive Model for the Design of Plasmonic Metal/Semiconductor Composite Photocatalysts. *ACS Catal.* **2011**, *1*, 1441−1447.
(18) Zheng, Z.; Huang, B.; Qin, X.; Zhang, X.; Dai, Y.; Whangbo, M. Facile in Situ Synthesis of Visible-Light Plasmonic Photocatalysts M@TiO_2 (M = Au, Pt, Ag) and Evaluation of Their Photocatalytic Oxidation of Benzene to Phenol. *J. Mater. Chem.* **2011**, *21*, 9079−9087.
(19) Ma, B.; Guo, J.; Dai, W.; Fan, K. Ag-AgCl/WO_3 Hollow Sphere with Flower-Like Structure and Superior Visible Photocatalytic Activity. *Appl. Catal., B* **2013**, *123*, 193−199.
(20) Zhu, M.; Chen, P.; Liu, M. Highly Efficient Visible-Light-Driven Plasmonic Photocatalysts Based on Graphene Oxide-Hybridized One-Dimensional Ag/AgCl Heteroarchitectures. *J. Mater. Chem.* **2012**, *22*, 21487−21494.
(21) Wang, P.; Huang, B.; Zhang, Q.; Zhang, X.; Qin, X.; Dai, Y.; Zhan, J.; Yu, J.; Liu, H.; Lou, Z. Highly Efficient Visible Light Plasmonic Photocatalyst Ag@Ag (Br, I). *Chem.—Eur. J.* **2010**, *16*, 10042−10047.
(22) Wang, P.; Huang, B.; Zhang, X.; Qin, X.; Jin, H.; Dai, Y.; Wang, Z.; Wei, J.; Zhan, J.; Wang, S. Highly Efficient Visible-Light Plasmonic Photocatalyst Ag@AgBr. *Chem.—Eur. J.* **2009**, *15*, 1821−1824.
(23) Wang, P.; Huang, B.; Lou, Z.; Zhang, X.; Qin, X.; Dai, Y.; Zheng, Z.; Wang, X. Synthesis of Highly Efficient Ag@AgCl Plasmonic Photocatalysts with Various Structures. *Chem.—Eur. J.* **2010**, *16*, 538−544.
(24) An, C.; Peng, S.; Sun, Y. Facile Synthesis of Sunlight-Driven AgCl: Ag Plasmonic Nanophotocatalyst. *Adv. Mater.* **2010**, *22*, 2570−2574.
(25) Tang, Y.; Jiang, Z.; Xing, G.; Li, A.; Kanhere, P. D.; Zhang, Y.; Sum, T. C.; Li, S.; Chen, X.; Dong, Z. Efficient Ag@ AgCl Cubic Cage Photocatalysts Profit from Ultrafast Plasmon-Induced Electron Transfer Processes. *Adv. Funct. Mater.* **2013**, *23*, 2932−2940.
(26) Chen, D.; Yoo, S. H.; Huang, Q.; Ali, G.; Cho, S. O. Sonochemical Synthesis of Ag/AgCl Nanocubes and Their Efficient Visible-Light-Driven Photocatalytic Performance. *Chem.—Eur. J.* **2012**, *18*, 5192−5200.
(27) Li, J.; Yang, W.; Ning, J.; Zhong, Y.; Hu, Y. Rapid Formation of AgnX (X = S, Cl, PO_4, C_2O_4) Nanotubes via an Acid-Etching Anion Exchange Reaction. *Nanoscale* **2014**, *6*, 5612−5615.
(28) Sang, Y.; Kuai, L.; Chen, C. Y.; Fang, Z.; Geng, B. Y. Fabrication of a Visible-Light-Driven Plasmonic Photocatalyst of $AgVO_3$@AgBr@ Ag Nanobelt Heterostructures. *ACS Appl. Mater. Interfaces* **2014**, *6*, 5061−5068.
(29) Yang, X.; Xue, H. T.; Xu, J.; Huang, X.; Zhang, J.; Tang, Y. B.; Ng, T. W.; Kwong, H. L.; Meng, X. M.; Lee, C. S. Synthesis of Porous ZnS:Ag_2S Nanosheets by Ion Exchange for Photocatalytic H_2 Generation. *ACS Appl. Mater. Interfaces* **2014**, *6*, 9078−9084.
(30) Cheng, H.; Huang, B.; Qin, X.; Zhang, X.; Dai, Y. A Controlled Anion Exchange Strategy to Synthesize Bi_2S_3 Nanocrystals/BiOCl Hybrid Architectures with Efficient Visible Light Photoactivity. *Chem. Commun.* **2011**, *48*, 97−99.
(31) Cheng, H.; Huang, B.; Wang, P.; Wang, Z.; Lou, Z.; Wang, J.; Qin, X.; Zhang, X.; Dai, Y. In Situ Ion Exchange Synthesis of the Novel Ag/AgBr/BiOBr Hybrid with Highly Efficient Decontamination of Pollutants. *Chem. Commun.* **2011**, *47*, 7054−7056.
(32) Zhang, S.; Li, J.; Zeng, M.; Li, J.; Xu, J.; Wang, X. Bandgap Engineering and Mechanism Study of Nonmetal and Metal Ions Codoped Carbon Nitride: C+ Fe as an Example. *Chem.—Eur. J.* **2014**, *20*, 9805−9812.
(33) Zhang, S.; Li, J.; Zeng, M.; Xu, J.; Wang, X.; Hu, W. Polymer Nanodots of Graphitic Carbon Nitride as Effective Fluorescent Probes for the Detection of Fe^{3+} and Cu^{2+} Ions. *Nanoscale* **2014**, *6*, 4157−4162.
(34) Zhang, S.; Li, J.; Zeng, M.; Zhao, G.; Xu, J.; Hu, W.; Wang, X. In Situ Synthesis of Water-Soluble Magnetic Graphitic Carbon Nitride Photocatalyst and Its Synergistic Catalytic Performance. *ACS Appl. Mater. Interfaces* **2013**, *5*, 12735−12743.
(35) Zhang, S.; Zhao, L.; Zeng, M.; Li, J.; Xu, J.; Wang, X. Hierarchical Nanocomposites of Polyaniline Nanorods Arrays on Graphitic Carbon Nitride Sheets with Synergistic Effect for Photocatalysis. *Catal. Today* **2014**, *224*, 114−121.
(36) Zhu, M.; Chen, P.; Liu, M. Graphene Oxide Enwrapped Ag/AgX (X = Br, Cl) Nanocomposite as a Highly Efficient Visible-Light Plasmonic Photocatalyst. *ACS Nano* **2011**, *5*, 4529−4536.
(37) Ma, T. Y.; Tang, Y.; Dai, S.; Qiao, S. Z. Proton-Functionalized Two-Dimensional Graphitic Carbon Nitride Nanosheet: An Excellent Metal-/Label-free Biosensing Platform. *Small* **2014**, *10*, 2382−2389.
(38) Wang, P.; Huang, B.; Qin, X.; Zhang, X.; Dai, Y.; Wei, J.; Whangbo, M. H. Ag@ AgCl: A Highly Efficient and Stable Photocatalyst Active under Visible Light. *Angew. Chem., Int. Ed.* **2008**, *47*, 7931−7933.
(39) Jiang, J.; Zhang, L. Rapid Microwave-Assisted Nonaqueous Synthesis and Growth Mechanism of AgCl/Ag, and Its Daylight-Driven Plasmonic Photocatalysis. *Chem.—Eur. J.* **2011**, *17*, 3710−3717.
(40) Zhang, X.; Xie, X.; Wang, H.; Zhang, J.; Pan, B.; Xie, Y. Enhanced Photoresponsive Ultrathin Graphitic-Phase C_3N_4 Nanosheets for Bioimaging. *J. Am. Chem. Soc.* **2013**, *135*, 18−21.
(41) Chen, D.; Li, T.; Chen, Q.; Gao, J.; Fan, B.; Li, J.; Li, X.; Zhang, R.; Sun, J.; Gao, L. Hierarchically Plasmonic Photocatalysts of Ag/AgCl Nanocrystals Coupled with Single-Crystalline WO_3 Nanoplates. *Nanoscale* **2012**, *4*, 5431−5439.
(42) Murdoch, M.; Waterhouse, G.; Nadeem, M.; Metson, J.; Keane, M.; Howe, R.; Llorca, J.; Idriss, H. The Effect of Gold Loading and Particle Size on Photocatalytic Hydrogen Production from Ethanol over Au/TiO_2 Nanoparticles. *Nat. Chem.* **2011**, *3*, 489−492.
(43) Kim, I. Y.; Park, S.; Kim, H.; Park, S.; Ruoff, R. S.; Hwang, S. J. Strongly-Coupled Freestanding Hybrid Films of Graphene and Layered Titanate Nanosheets: An Effective Way to Tailor the Physicochemical and Antibacterial Properties of Graphene Film. *Adv. Funct. Mater.* **2014**, *24*, 2288−2294.

(44) Buriak, J. M.; Kamat, P. V.; Schanze, K. S. Best Practices for Reporting on Heterogeneous Photocatalysis. *ACS Appl. Mater. Interfaces* **2014**, *6*, 11815−11816.
(45) Ye, L.; Liu, J.; Gong, C.; Tian, L.; Peng, T.; Zan, L. Two Different Roles of Metallic Ag on Ag/AgX/BiOX (X = Cl, Br) Visible Light Photocatalysts: Surface Plasmon Resonance and Z-Scheme Bridge. *ACS Catal.* **2012**, *2*, 1677−1683.